JOURNAL OF MATERIALS SCIENCE **38** (2003) 377–388

Dihedral angle measurement in microgravity liquid phase sintered microstructures

S. YE, Y. HE, J. E. SMITH, JR.
Consortium for Materials Development in Space and Department of Chemical and Materials Engineering, University of Alabama in Huntsville, Huntsville, AL 35899, USA
E-mail: jesmith@che.uah.edu

Liquid phase sintered materials are characterized by a connected microstructure composed of contacting grains in a solidified matrix phase. Characterizations on the sintered microstructure are typically performed by two-dimensional cross sections. A new dihedral angle model based totally on the geometry of the spherical solid grains without any further assumptions is presented in this paper to determine the dihedral angles measured in two-dimensional sections vs. the dihedral angles in three dimensions. The result shows that the average dihedral angle measured on sections is 14/15 the dihedral angle in three dimensions. The expected frequencies of the simulation are favorably compared with the experimental results obtained from microgravity liquid phase sintered Fe-Cu alloys with four different solid volume fractions (50, 60, 70, 80 vol% Fe balanced with Cu) and six different sintering times (10, 20, 30, 40, 60 and 330 minutes) when a 3-D dihedral angle with a standard deviation of 10°, in our case, $40^\circ \pm 10^\circ$, was employed in the model. The goodness of fit of the theoretical 2-D results with the experimental data was determined by chi-squared test. The fit of the data is good since all the computed values of χ^2 are smaller than the critical value.

1. Introduction

The dihedral angle is important to the microstructure of polycrystalline grains and to grain-grain contacts in the liquid phase. It determines the equilibrium size of the contact between grains and affects both the liquid and grain shapes. From Young's Equation

$$\cos\left(\frac{\phi}{2}\right) = \frac{\gamma_{SS}}{2\gamma_{SL}} \tag{1}$$

where ϕ is the dihedral angle, γ_{SS} is the solid-solid grain boundary energy, and γ_{SL} is the solid-liquid interface energy, a calculation of the relative energies is only possible if an accurate measurement of the dihedral angle is made.

A classic problem in analyzing microstructures is to convert from a typical two-dimensional metallographic cross section to a true representation of the underlying three-dimensional microstructure [1]. Many efforts have been focused on that conversion [2–4]. The dihedral angle conversion is one of the problems because the dihedral angle ϕ is formed where a solid-solid grain boundary intersects the liquid [5], it involves two planes in three dimensions, and only a two-dimensional cut through the dihedral angle is observed.

A typical two-dimensional metallographic section is shown in Fig. 1. The microstructure is composed of Fe grains and a penetrating matrix of Fe-Cu alloy. During sintering, the Fe grains were solid and the matrix alloy was liquid. On two-dimensional micrographs, because grain contacts are at random orientations to any cross section cut through the experimental specimen, a distribution of observed dihedral angles results, represented in the proportions of their inherent probabilities [6]. This distribution must then be manipulated to obtain a single "true or effective" dihedral angle.

Dihedral angles measured by the statistical method were first employed by Harker and Parker [6]. They developed a method for obtaining a single 3-D dihedral angle from the distribution of 2-D angles that result from random sectioning of an angle. They developed the following equation to relate the calculated 2-D distribution and a specific 3-D dihedral angle

$$\tan\gamma = \frac{2\sin\phi\cos\theta}{\sin^2\theta(\cos 2\varphi - \cos\phi) + 2\cos\phi} \tag{2}$$

where ϕ is the true dihedral angle, γ is the observed angle, and θ and φ are polar coordinates. The cumulative frequencies of the theoretically expected dihedral angle distributions were compared with the experimentally measured angles assuming that a specimen's grain structure consists of a network of grain edges that are randomly oriented and uniformly distributed. However, the peaks observed at the modal angle of experimental data were blunter and broader than expected from the model. No good fits in the literature could be found. The major reason for the discrepancy in the distributions calculated from Equation 2 is the presence of a range of dihedral angles in all specimens [7, 8].

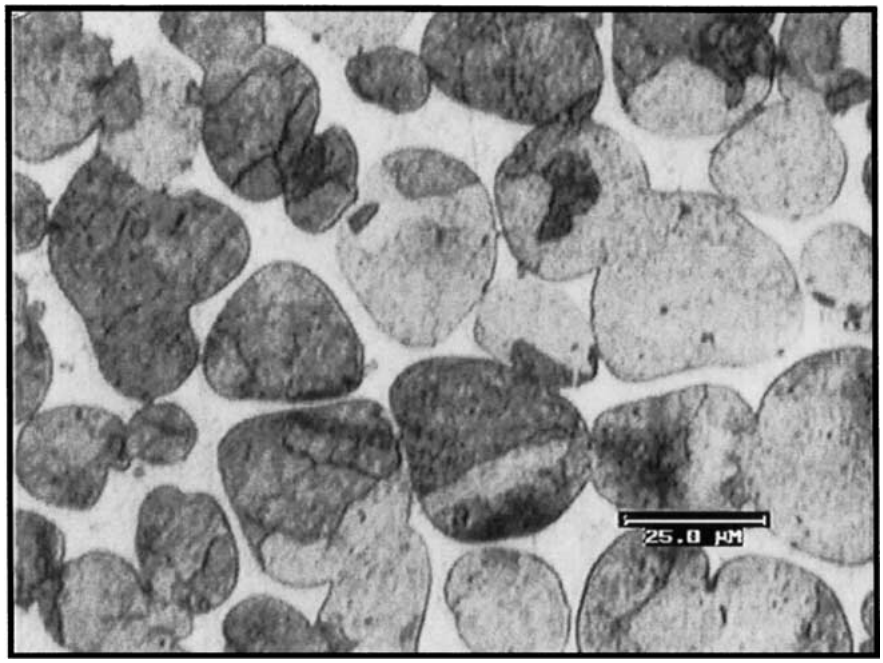

Figure 1 Micrograph of a liquid phase sintered Fe-Cu alloy (60 vol% Fe/Cu) sintered at 1150°C for 60 minutes, different dihedral angles were shown.

A distribution in the dihedral angle can result from varying grain boundary energy with misorientation, anisotropic surface energies and various misorientation angles, or even measuring error [8].

Riegger and Van Vlack [9] showed that the median dihedral as measured on two-demensional sections provides a satisfactory value for dihedral angle determination with a typical error of 5°. Factors, such as grain size distribution and spherical grain shape, have never been considered in the previous model. Further consideration of these factors is a goal of this paper.

2. Mathematical model

In the space with Cartesian coordinates, a vector **V** can be expressed as

$$\mathbf{V} = A\mathbf{i} + B\mathbf{j} + C\mathbf{k} \tag{3}$$

where A, B and C are the ordinates of the vector **V** at X, Y and Z coordinates, as shown in Fig. 2. This vector can also be described using Spherical coordinates (r, θ, φ), which are related to the Cartesian coordinates by

$$\begin{aligned} A &= r\sin\theta\cos\varphi \\ B &= r\sin\theta\sin\varphi \\ C &= r\cos\theta \end{aligned} \tag{4}$$

Here, r is the length of the vector **V**. If this vector $\mathbf{V} = \langle A, B, C\rangle$ is a normal line of the plane containing the point (x_1, y_1, z_1), the plane perpendicular to it can be represented, in a standard form, by the equation

$$A(x - x_1) + B(y - y_1) + C(z - z_1) = 0 \tag{5}$$

That is,

$$Ax + By + Cz - Ax_1 - By_1 - Cz_1 = 0 \tag{6}$$

In this way, the sectioning plane, P_1, which passes through the point (A, B, C) and is normal to the vector **V** (Fig. 3), can be expressed as

$$Ax + By + Cz - A^2 - B^2 - C^2 = 0 \tag{7}$$

or

$$Ax + By + Cz - r^2 = 0 \tag{8}$$

Substituting Equation 4 into Equation 8, the plane P_1 can be expressed by the following equation:

$$(\sin\theta\cos\varphi)x + (\sin\theta\sin\varphi)y + (\cos\theta)z - r = 0 \tag{9}$$

The cross section formed by the plane, P_1, intersecting the spherical solid grain as shown in Fig. 3 is a circular area C_1 and is determined by combining the plane Equation 9 and the following sphere Equation 10

$$x^2 + y^2 + z^2 = R_1^2 \tag{10}$$

where R_1 is the radius of the spherical grain.

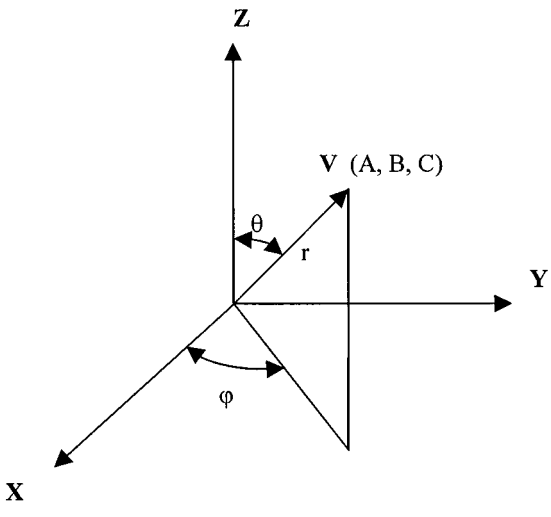

Figure 2 Cartesian coordinates and spherical coordinates.

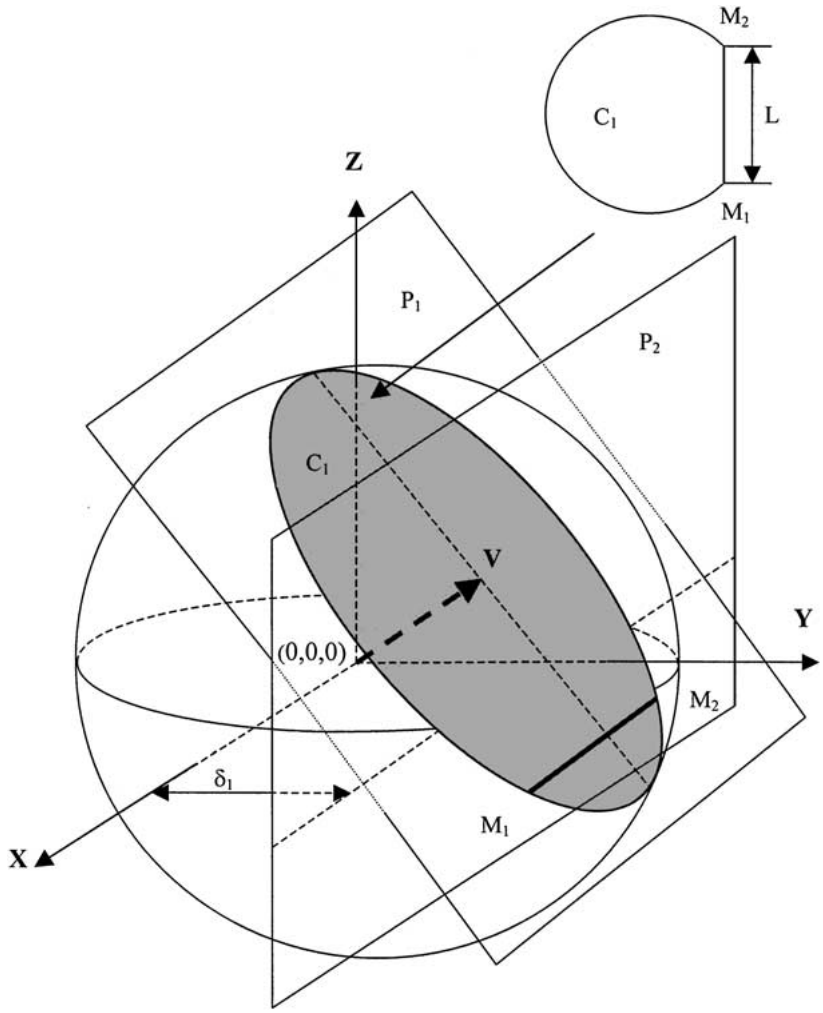

Figure 3 An ideal model of a solid grain with sectioning planes.

The other plane, P_2, in Fig. 3 is a plane normal to Y coordinate (parallel to the plane XZ). Its equation is given by

$$y = \delta_1 \tag{11}$$

where δ_1 is the distance from the origin to the plane P_2.

The intersection of the circular area C_1 and the plane P_2 forms a straight line M_1M_2. Thus, the ends of Line M_1M_2 can be determined by solving Equations 9, 10 and 11.

Substituting Equation 11 into Equation 9 of Plane 1, the variable z can be written as

$$z = -(\tan\theta\cos\varphi)x + r\sec\theta - \delta_1\tan\theta\sin\varphi \tag{12}$$

Substituting Equations 11 and 12 into Equation 10 of a sphere, one gets

$$\begin{aligned}(1 + \tan^2\theta\cos^2\varphi)x^2 - 2(\tan\theta\cos\varphi)\\ \times (r\sec\theta - \delta_1\tan\theta\sin\varphi)x\\ + (r\sec\theta - \delta_1\tan\theta\sin\varphi)^2 - R_1^2 + \delta_1^2 = 0\end{aligned} \tag{13}$$

The solution of Equation 13 is

$$x_{1,2} = \frac{2(\tan\theta\cos\varphi)(r\sec\theta - \delta_1\tan\theta\sin\varphi) \pm \Delta}{2(1 + \tan^2\theta\cos^2\varphi)} \tag{14}$$

where

$$\Delta = 2\sqrt{(R_1^2 - \delta_1^2)(1 + \tan^2\theta\cos^2\varphi) - (r\sec\theta - \delta_1\tan\theta\sin\varphi)^2} \tag{15}$$

From Equation 14, we have

$$x_1 - x_2 = \frac{\Delta}{1 + \tan^2\theta\cos^2\varphi} \tag{16}$$

Considering Equation 12, it can be shown that

$$z_1 - z_2 = -(\tan\theta\cos\varphi)(x_1 - x_2) = -\frac{(\tan\theta\cos\varphi)\Delta}{1 + \tan^2\theta\cos^2\varphi} \tag{17}$$

After two points M_1 (x_1, δ_1, z_1) and M_2 (x_2, δ_1, z_2) are known, the length of the line M_1M_2 is expressed as

$$L = |M_1 - M_2| \tag{18}$$

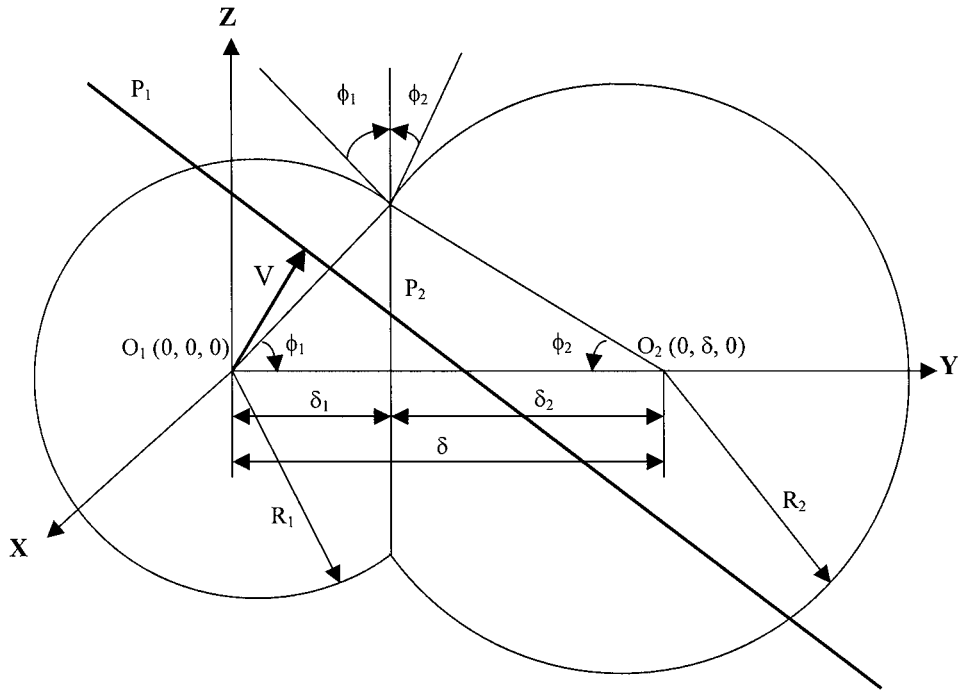

Figure 4 The model of two solid grains, showing the major calculation parameters.

Substituting Equations 16 and 17 into Equation 18, the length, L, of the line can be calculated by

$$L = \sqrt{(x_1 - x_2)^2 + (z_1 - z_2)^2} = \frac{\Delta}{\sqrt{(1 + \tan^2\theta\cos^2\varphi)}} \tag{19}$$

Fig. 4 sketches a schematic geometry of these two solid grains in contact to form a three dimensional dihedral angle ϕ. Set Plane P_2 to be the contact plane of two solid grains with radii R_1 and R_2. No matter where the sectioning plane, P_1, is, the following relationships always hold,

$$\delta_1 = R_1\cos\phi_1 \tag{20}$$

$$R_1\sin\phi_1 = R_2\sin\phi_2 \tag{21}$$

Thus, Δ can be further simplified to be

$$\Delta = 2\sqrt{R_1^2\sin^2\phi_1(1 + \tan^2\theta\cos^2\varphi) - (r\sec\theta - R_1\tan\theta\sin\varphi\cos\phi_1)^2} \tag{22}$$

$$\phi_2 = \sin^{-1}\left(\frac{R_1}{R_2}\sin\phi_1\right) \tag{23}$$

$$\cos\phi_2 = \sqrt{1 - \left(\frac{R_1}{R_2}\sin\phi_1\right)^2} \tag{24}$$

The dihedral angle of the grains in the three-dimensional space is

$$\phi = \phi_1 + \phi_2 = \phi_1 + \sin^{-1}\left(\frac{R_1}{R_2}\sin\phi_1\right) \tag{25}$$

that is,

$$\sin(\phi - \phi_1) = \frac{R_1}{R_2}\sin\phi_1 \tag{26}$$

Equation 26 can be rewritten as

$$\sin\phi\cos\phi_1 - \cos\phi\sin\phi_1 - \frac{R_1}{R_2}\sin\phi_1 = 0 \tag{27}$$

Thus,

$$\tan\phi_1 = \frac{R_2\sin\phi}{R_2\cos\phi + R_1} \tag{28}$$

Also,

$$\sin\phi_1 = \frac{R_2\sin\phi}{\sqrt{R_1^2 + R_2^2 + 2R_1R_2\cos\phi}} \tag{29}$$

$$\cos\phi_1 = \frac{R_2\cos\phi + R_1}{\sqrt{R_1^2 + R_2^2 + 2R_1R_2\cos\phi}} \tag{30}$$

The distance between the two grain centers is determined by

$$\begin{aligned}\delta &= R_1\cos\phi_1 + R_2\cos\phi_2 \\ &= \sqrt{R_1^2 + R_2^2 - 2R_1R_2\cos(\pi - \phi)} \\ &= \sqrt{R_1^2 + R_2^2 + 2R_1R_2\cos\phi}\end{aligned} \tag{31}$$

Substituting Equations 22, 29, 30 and 31 into Equation 19, we have

$$L = 2\sqrt{\frac{R_1^2 R_2^2 \sin^2\phi(1+\tan^2\theta\cos^2\varphi) - [r\delta\sec\theta - R_1\tan\theta\sin\varphi(R_2\cos\phi + R_1)]^2}{\delta^2(1+\tan^2\theta\cos^2\varphi)}} \tag{32}$$

where δ is defined in Equation 31.

From the definition of L, the length of the intersection line of sectioning plane, P_1, and the intergrain contact plane, P_2, L is a function of the position of the random sectioning plane, P_1 (r, θ, φ), the spherical grain sizes (R_1, R_2), and the three dimensional dihedral angle ϕ between the two grains. That is the length of the intersection of planes P_1 and P_2 varies with different sectioning plane position for the same grains and dihedral angle. Furthermore, the intersection of the sectioning plane and the two grains in contact is two circular areas in contact, as shown in Fig. 5, for a meaningful two-dimensional dihedral angle to be observed. Here, C_1 and C_2 are the intersection area of the plane P_1 with two grains, respectively.

The radius of the circular area C_1 is given by

$$r_1 = \sqrt{R_1^2 - r^2} \tag{33}$$

The distance from the point O_2 $(0, \delta, 0)$ to the sectioning plane, P_1, can be calculated by

$$\begin{aligned} r' &= |(\sin\theta\sin\varphi)0 + (\sin\theta\cos\varphi)\delta + (\cos\theta)0 - r| \\ &= \left|\sqrt{R_1^2 + R_2^2 + 2R_1R_2\cos\phi}\sin\theta\sin\varphi - r\right| \end{aligned} \tag{34}$$

Therefore, the radius of circular area C_2 is

$$\begin{aligned} r_2 &= \sqrt{R_2^2 - r'^2} \\ &= \sqrt{R_2^2 - \left(\sqrt{R_1^2 + R_2^2 + 2R_1R_2\cos\phi}\sin\theta\sin\varphi - r\right)^2} \end{aligned} \tag{35}$$

Fig. 6 is a two-dimensional projection on the sectioning plane of the two three-dimensional solid grains in contact. Similar to Equations 21 and 23, we have

$$r_1\sin\gamma_1 = r_2\sin\gamma_2 \tag{36}$$

and

$$\gamma_2 = \sin^{-1}\left(\frac{r_1}{r_2}\sin\gamma_1\right) \tag{37}$$

Therefore, the observed two-dimensional dihedral angle, which is the sum of angles γ_1 and γ_2 in Fig. 6, is given by

$$\gamma = \gamma_1 + \gamma_2 = \gamma_1 + \sin^{-1}\left(\frac{r_1}{r_2}\sin\gamma_1\right) \tag{38}$$

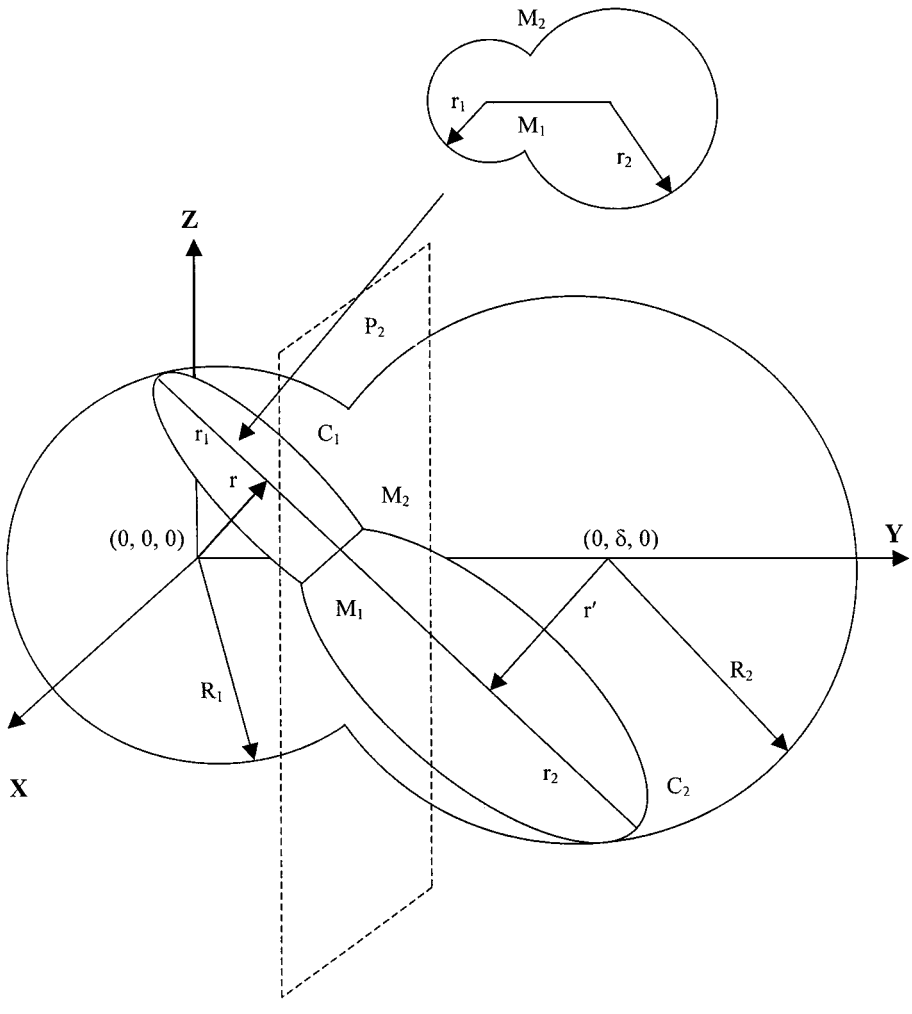

Figure 5 A plane sectioned the two three-dimensional solid grains in contact.

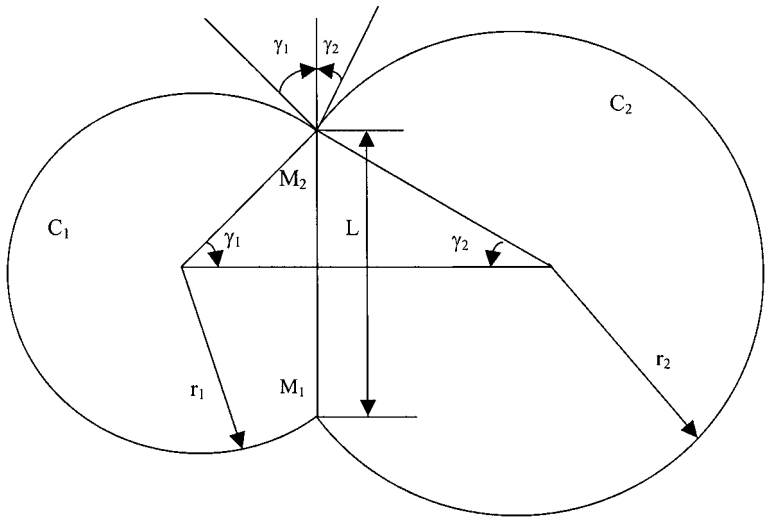

Figure 6 A two-dimensional image of the two three-dimensional solid grains in contact.

where

$$\gamma_1 = \sin^{-1}\left(\frac{L}{2r_1}\right) = \sin^{-1}\sqrt{\frac{R_1^2R_2^2\sin^2\phi(1+\tan^2\theta\cos^2\varphi) - \left[r\delta\sec\theta - R_1\tan\theta\sin\varphi(R_2\cos\phi + R_1)\right]^2}{\left(R_1^2 - r^2\right)\delta^2(1+\tan^2\theta\cos^2\varphi)}} \tag{39}$$

and

$$\gamma_2 = \sin^{-1}\left(\frac{L}{2r_2}\right) = \sin^{-1}\left(\frac{r_1}{r_2}\sin\gamma_1\right) = \sin^{-1}\sqrt{\frac{R_1^2R_2^2\sin^2\phi(1+\tan^2\theta\cos^2\varphi) - \left[r\delta\sec\theta - R_1\tan\theta\sin\varphi(R_2\cos\phi + R_1)\right]^2}{\left[R_2^2 - (\delta\sin\theta\sin\varphi - r)\right]^2\delta^2(1+\tan^2\theta\cos^2\varphi)}} \tag{40}$$

r_1, r_2, and γ are the characterizations which we can observe and measure directly on a two dimensional sectioning plane.

3. Simulation technique

First, we consider equal sized solid grains. Consider two equal sized solid grains contact in space, as illustrated in Fig. 4. The radii of the solid grains expressed by Equations 33 and 35 and the length of the contact neck given in Equation 32 on the two-dimensional sectioning plane can be simplified as the following,

$$r_1 = R\sqrt{1 - r_0^2} \tag{41}$$

$$r_2 = R\sqrt{1 - \left(2\cos\frac{\phi}{2}\sin\theta\sin\varphi - r_0\right)^2} \tag{42}$$

$$L = 2R\sqrt{\sin^2\frac{\phi}{2} - \frac{\left(r_0\sec\theta - \tan\theta\sin\varphi\cos\frac{\phi}{2}\right)^2}{1+\tan^2\theta\cos^2\varphi}} \tag{43}$$

where R is the radius of the solid grain, and r_0 is a random normalized vector length given by

$$r_0 = \frac{r}{R} \tag{44}$$

The two-dimensional dihedral angle is expressed as

$$\gamma = \sin^{-1}\left(\frac{L}{2r_1}\right) + \sin^{-1}\left(\frac{L}{2r_2}\right) = \sin^{-1}\sqrt{\frac{1}{1-r_0^2}\left[\sin^2\frac{\phi}{2} - \frac{\left(r_0\sec\theta - \tan\theta\sin\varphi\cos\frac{\phi}{2}\right)^2}{1+\tan^2\theta\cos^2\varphi}\right]} + \sin^{-1}\sqrt{\frac{1}{1-\left(2\cos\frac{\phi}{2}\sin\theta\sin\varphi - r_0\right)^2}\left[\sin^2\frac{\phi}{2} - \frac{\left(r_0\sec\theta - \tan\theta\sin\varphi\cos\frac{\phi}{2}\right)^2}{1+\tan^2\theta\cos^2\varphi}\right]} \tag{45}$$

The three variables of Spherical coordinates, the normalized length of the vector, r_0, and the two space angles, θ and φ are the calculation parameters for a given ϕ, the three-dimensional dihedral angle.

Then, in order to investigate the influence of the grain size distribution to the observed dihedral angles on the two-dimensional sectioning planes, different grain sizes of R_1 and R_2 are considered through a parameter λ defined as

$$\lambda = \frac{R_2}{R_1} \tag{46}$$

From the definition of Equation 46, Equations 32, 33, and 35 was rewritten as

$$r_1 = R_1\sqrt{1 - r_{01}^2} \tag{47}$$

$$r_2 = R_1\sqrt{\lambda^2 - (\delta_\lambda \sin\theta \sin\varphi - r_{01})^2} \tag{48}$$

$$L = 2R_1\sqrt{\frac{\lambda^2 \sin^2\phi(1 + \tan^2\theta\cos^2\varphi) - [r_{01}\delta_\lambda \sec\theta - \tan\theta \sin\varphi(\lambda\cos\phi + 1)]^2}{(1 + \tan^2\theta\cos^2\varphi)\delta_\lambda^2}} \tag{49}$$

where R_1 is the radius of the left solid grain, R_2 is the radius of the right solid grain in Fig. 4, and r_{01} is a random normalized vector length given by

$$r_{01} = \frac{r}{R_1} \tag{50}$$

δ_λ is a dimensionless distance between the two grain centers

$$\delta_\lambda = \frac{\delta}{R_1} = \sqrt{1 + \lambda^2 + 2\lambda\cos\phi} \tag{51}$$

The observed dihedral angle is expressed as

$$\begin{aligned}\gamma &= \sin^{-1}\left(\frac{L}{2r_1}\right) + \sin^{-1}\left(\frac{L}{2r_2}\right) \\ &= \sin^{-1}\sqrt{\frac{\lambda^2 \sin^2\phi(1 + \tan^2\theta\cos^2\varphi) - [r_{01}\delta_\lambda \sec\theta - \tan\theta \sin\varphi(\lambda\cos\phi + 1)]^2}{\left(1 - r_{01}^2\right)(1 + \tan^2\theta\cos^2\varphi)\delta_\lambda^2}} \\ &+ \sin^{-1}\sqrt{\frac{\lambda^2 \sin^2\phi(1 + \tan^2\theta\cos^2\varphi) - [r_{01}\delta_\lambda \sec\theta - \tan\theta \sin\varphi(\lambda\cos\phi + 1)]^2}{\left[\lambda^2 - (\delta_\lambda \sin\theta \sin\varphi - r_{01})^2\right](1 + \tan^2\theta\cos^2\varphi)\delta_\lambda^2}}\end{aligned} \tag{52}$$

The three variables of Spherical coordinates, the normalized length of the vector, r_{01}, and the two space angles, θ and φ are the calculation parameters for a given ϕ and λ.

In both the mathematical model and the simulation, the left grain in Fig. 4 is centered at the origin (0, 0, 0) with a radius R (or R_1). The center of the right-hand grain is located at a distance δ from the origin and is of the same radius (or R_2). Both grains are spheres. A two-dimensional cross section is generated when a plane sections either of the grains physically. In general, two important factors must be considered in the simulation: the randomness of a sectioning plane and the effectiveness of this sectioning plane.

The random vector is generated by creating three random variables: the length of the vector, r, and two space angles, θ and φ. Usually, the three variables are assumed to distribute uniformly within a given range. Such a vector can be considered as one variable in space. The sectioning plane is defined normal to the vector, passing through the end point of the vector. A mathematically possible sectioning plane is generated through the combination of these three variables.

Not all planes given by the various mathematical combinations of these three variables exist physically in the real world. For example, some possible sectioning planes have no intersections with either of the two grains. It is necessary to check the effectiveness of the sectioning planes before we count this sectioning. This is done as follows.

First, for a given combination of these three variables, compute the quantities of r_1^2, r_2^2 and L^2 by Equations 41–43 (or Equations 47–49). Second, this combination is considered to form a physically possible sectioning plane only if the following conditions are satisfied simultaneously,

$$r_2^2 \geq 0 \tag{53}$$

$$L^2 \geq 0 \tag{54}$$

$$\frac{L^2}{4r_1^2} \leq 1 \tag{55}$$

$$\frac{L^2}{4r_2^2} \leq 1 \tag{56}$$

A large number of sections is needed to cover all the possible sectioning planes that may occur in an experiment. For example, for a 3-D dihedral angle of 20°, 40,000 sectioning planes are needed to get more than 5,000 effective sectioning planes. A large number of effective sectioning planes guarantees the randomness of the section and the correctness of the statistical result.

The simulation procedure is summarized as follows:

1. Randomly create a vector $\mathbf{V}$ (r, θ, φ),
2. Generate the sectioning plane P_1 which is normal to the vector $\mathbf{V}$ based on Equation 9,

3. For a given λ and three-dimensional dihedral angle, calculate the theoretically predicted dihedral angle and grain sizes using Equations 41–43 or 47–49,

4. Check the effectiveness of the sectioning plane using Equations 53–56,

5. Repeat the above steps as many as needed,

6. Compute the mean values of the theoretically predicted dihedral angle and the grain sizes or the distributions of the dihedral angle and the grain sizes.

The first set of equations, Equations 41–43, developed here can be used to verify the derivation of the second set, Equations 47–49, as we'll show in the next section.

4. Results and discussions

4.1. Relation between the 2-D grain radius and the equal sized 3-D grain radius

The relationship between the arithmetic mean of the two-dimensional grain radius and the equal sized three-dimensional grain radius can be easily obtained from Equation 41 by integrating

$$\sqrt{1-r_0^2} \quad \text{from} \quad r_0 = 0 \quad \text{to} \quad r_0 = 1,$$

that is

$$\bar{r}_1 = \frac{\pi}{4} R \tag{57}$$

The measured grain size depends linearly on the space grain size. The coefficient $\pi/4$ [3] is obtained at a constant probability of cutting a sphere in a distance r from the center $r = 0$ to the surface $r = R$. This is true if the grain has no relation to neighboring grains and the grain size is the only concern of the section. Simulation using a uniformly distributed random r_0, between 0 and 1 gives an answer of 0.785 when the number of cutting planes is large enough. A number of 100,000 was used in this simulation. The frequencies of the sections at various normalized intersect radii is shown in Fig. 7. It can be seen in this figure that more than 40% of the sections intersect the center of the grains. This means that any sectioning plane cutting through a specimen with equal sized spherical grains will intersect over 40% of the grain centers.

The relationships between the mean of the two-dimensional grain sizes and the equal sized grains in three-dimensional space are also linear when the sectioning plane intersects two grains in contact, as shown in Fig. 5. The average correlation coefficient is 0.8811 for both r_1 and r_2 with dihedral angles ranging from 15° to 75° typical for most liquid phase sintered materials [1]. This is about 12 percent larger than $\pi/4$ calculated from the arithmetic mean of the intersect radii for a single grain. The equalization of the correlation coefficients for r_1 and r_2 also supports our model and simulation procedure. A larger coefficient is expected, since the effective sections counted this time must also have an observable dihedral angle in the simulation. The geometrical limitation for two grains in contact with an observable dihedral angle results in a non-constant probability of sectioning a sphere at a distance r from the center between $r = 0$ and $r = R$. The probability of cutting a grain near $r = R$, that is the corresponding grain sizes, r_1, r_2, near 0, is very sparse and rare from this geometrical consideration as we can see in Fig. 7. Sixty five percent of the sections intersect the center of the equal sized spherical grains at a 3-D dihedral angle of 40°. The frequencies at various normalized intersect radii are different at various 3-D dihedral angles. At a 3-D dihedral angle of 80°, the frequency of sectioning through the grain centers decreases to 59%.

The correlation coefficients for r_1 and r_2 decrease as the 3-D dihedral angle is increased from 15° to 75°. This is because the intergrain contact area is increasing at a larger 3-D dihedral angle, and the larger contact area permits sections closer to $r = R$ (r_1, r_2 near 0) still reveal an observable dihedral angle. Thus, the mean ratio of r/R becomes smaller with an increasing dihedral angle. The correlation coefficient mentioned here is not a conversion coefficient since on a polished section plane, there always exist grains that are not in contact with any other grains. Fig. 8 shows the correlation coefficient as a function of the 3-D dihedral angle. The 3-D dihedral angle affect the grain size on an effective sectioning plane of the grains that reveals an observable dihedral angle.

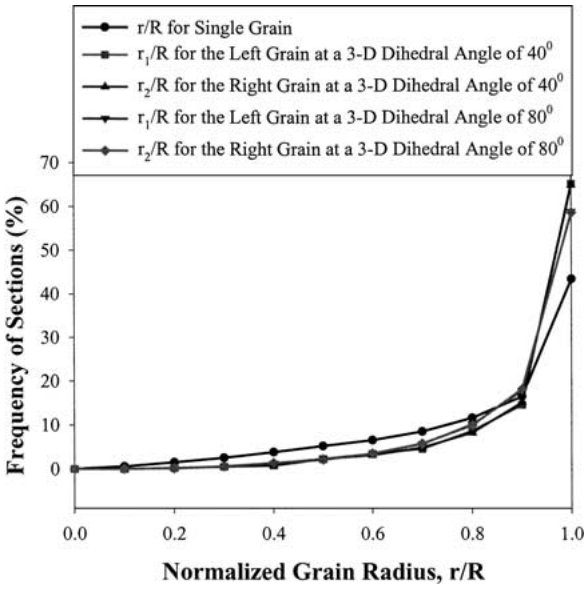

Figure 7 The occurrence of sectioning at different normalized grain radius.

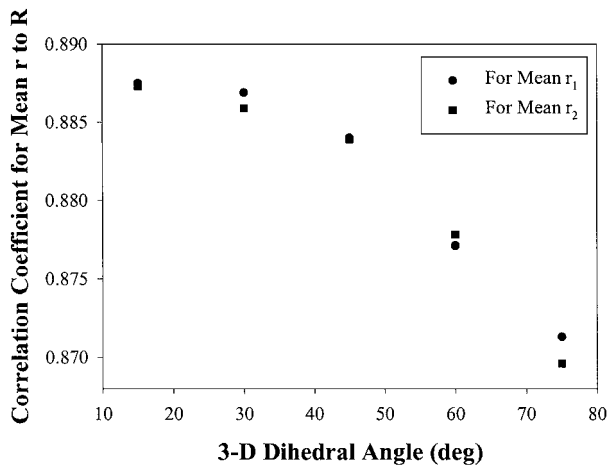

Figure 8 The mean simulated 2-D grain radii to the 3-D grain radius as a function of the 3-D dihedral angle.

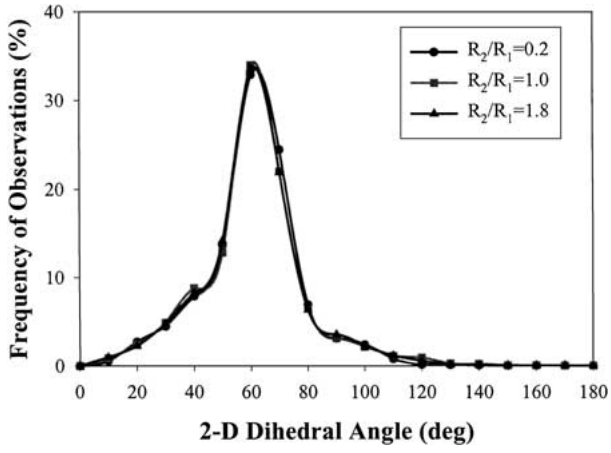

Figure 9 The effect of radius ratio of the two solid grains on the occurrence of observations of the 2-D dihedral angles at a 3-D dihedral angle of 60°.

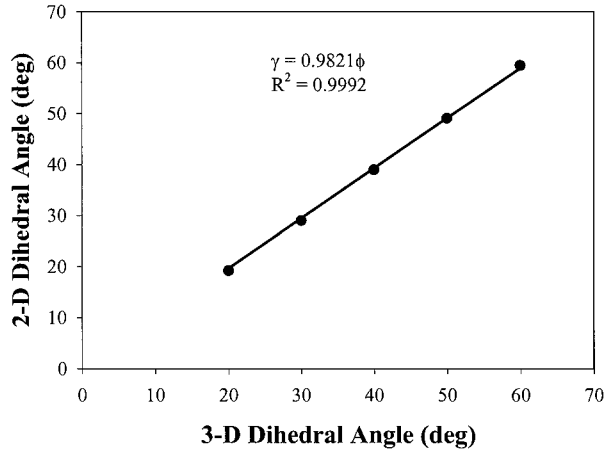

Figure 10 The theoretically expected mean of the 2-D dihedral angles as a function of the 3-D dihedral angles when the cutting planes are generated in the right half of the left grain.

4.2. Effect of grain size

The effect of grain size on the expected dihedral angle is shown in Fig. 9. The same mean and distribution of the expected dihedral angles were obtained under three different ratios of grain radii, 0.2, 1.0 and 1.8. These grain size ratios were randomly chosen between the typical normalized grain radii 0 to 2 in LSEM grain size distributions that fit our microgravity liquid phase sintered Fe-Cu samples [10]. The unequal grain sizes have no effect on the expected dihedral angles, at least when the grains are spherical. Thus, biased sampling will not be a problem if a sizable fraction of the particles seen in a polished plane cannot be measured with the best magnification available as discussed in [7]. Because no matter how different the grain sizes, the grain size distributions and the magnifications are, the typical ratio of the grain radii should be between 0 and 2. That is, in a microstructure composed of spherical solid grains dispersing in a liquid matrix, the 2-D dihedral angle is a function of the 3-D dihedral angle only.

As we can see in Fig. 9, depending on the position of the sectioning plane, the expected dihedral angle distributes between 0° and 180° with its peak on the 3-D dihedral angle (60° in Fig. 9) used to evaluate the expected dihedral angles. Both Equations 45 and 52 were used to compute the expected dihedral angles under the same conditions to verify the correctness of the derivation. The result of Equation 52 when $\lambda = 1$ is chosen to compute the expected dihedral angles is the same as the result obtained from Equation 45. This confirms the correctness of the derivation.

4.3. Relation between the 2-D dihedral angle and the 3-D dihedral angle

As the grain size distribution has no effect on the expected dihedral angles, Equation 45 was employed to simulate the relationship between the dihedral angle of solid grains in three-dimensional space and the corresponding dihedral angles on the two-dimensional plane. When only the sectioning planes generated in the right half of the grain that is centered in the origin are considered, the difference between the 3-D and 2-D dihedral angles is very small. The maximum difference is 1°, which is less than the 5° measurement error. For instance, for a 3-D dihedral angle of 60°, the mean value of the expected two-dimensional dihedral angles is 59.5°, which is very close to the actual dihedral angle in space. Fig. 10 shows the result of the simulation obtaining from the planes generated in the right half of the left grain. A conclusion that $\gamma = \phi$ is reasonable considering the random measurement error. This result was concluded by DeHoff [11] and is the result of Harker and Parker's equation because only half of the sphere was taken into account in their equation [6]. This can be clearly seen from Equation 2. Since $\cos 2\varphi$ gives the same mean values with $2\varphi = 2\pi r_0$ and $2\varphi = 4r_0$, r_0 is a random number between 0 and 1, Harker and Parker considered the sections and the resulted dihedral angles symmetric for the other half sphere in their model. This symmetry could hold if suitable coordinates or the right range of φ is chosen, for example, if φ is $-\pi/2$ to $\pi/2$.

In the model established specifically for dispersed solid grains, it is obvious that the left and right halves of the grain are not symmetric to generate a meaningful sectioning plane and an effective dihedral angle. The correlation coefficients, r_1/R and r_2/R, for the two grains are not the same either, if only the right half of the left grain is used for the simulation. The coefficient for the right grain is about 3% larger than that of the left one. The number of effective sectioning planes generated in the left half as described in Section 2 is much less than generated in the right half. However, the probability of a plane generated in the left half exists. Thus, the whole grain is taken into account to get an actual mean and distribution of the expected dihedral angles.

Smaller mean dihedral angles were obtained when the planes generated in the whole grain are used in the simulation. The result is shown in Fig. 11. From this figure, every 15° increase in the 3-D dihedral angle results in a loss of 1° in the mean value of the 2-D expected dihedral angles, that is, $\gamma = \frac{14}{15}\phi$. For a 60° 3-D dihedral angle, the expected 2-D dihedral angle is about 56°. The experimentally determined 2-D results for Fe-Cu samples processed in microgravity have a measured dihedral angle around 37.5° (Fig. 12), the actual 3-D dihedral angle should be 40° based on the simulation.

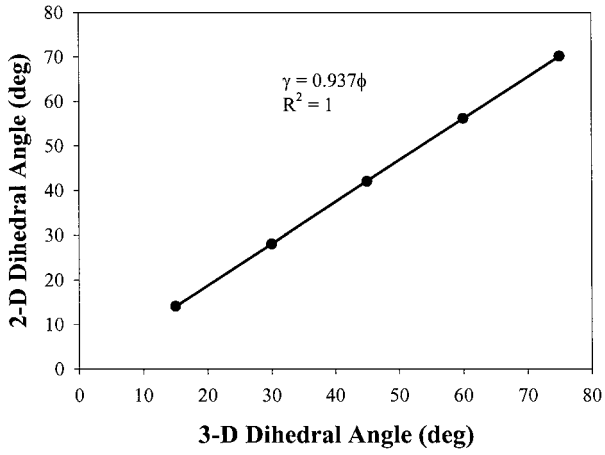

Figure 11 The theoretically expected mean of the 2-D dihedral angles as a function of the 3-D dihedral angles when the cutting planes are generated in the whole grain.

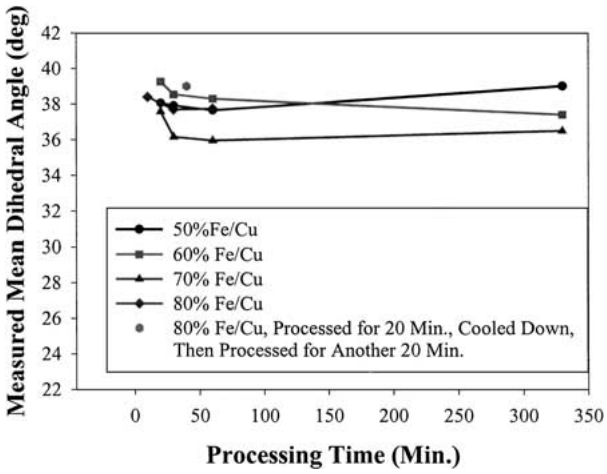

Figure 12 The experimentally measured 2-D dihedral angles.

4.4. Dihedral angle distribution

Fig. 13 shows the frequency of observations versus the 2-D dihedral angles at various 3-D dihedral angles of 20°, 40°, 60°, and 80°, respectively. As the 3-D dihedral angle increases, the distribution expands and the peak of the distribution decreases.

From the statistical point of view, the experimentally measured dihedral angle of a large number of 2-D measurements forms a distribution. The experimental dihedral angle distributions for more than 600 measurements in each specimen were established under various compositions and sintering times. There is no significant difference between the experimental dihedral angle distributions of the four compositions and the six sintering times. Agglomeration under microgravity is believed to promote an equilibrium particle configuration early on in microgravity liquid phase sintering [10]. However, difference between distributions of 50–70 vol% Fe/Cu and 80 vol% Fe/Cu exists. The peak occurrence of the experimental dihedral angles is 30° for 50–70 vol% Fe/Cu, while the peak for 80 vol% Fe/Cu is 40°. Two typical experimental distributions are shown in Figs 14 and 15 respectively. The mean values of the dihedral angles for 80 vol% Fe/Cu are almost the same as the other compositions as we can see in Fig. 12, although the higher solid volume fraction moves the peak of the dihedral angle distribution to a bigger angle.

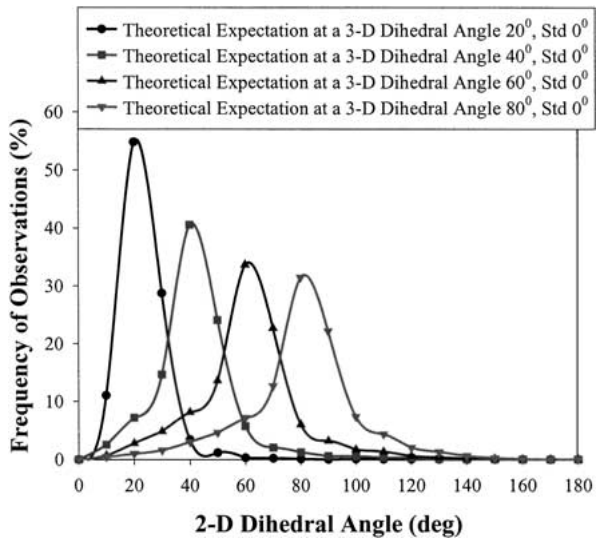

Figure 13 Theoretical frequency of observations of the 2-D dihedral angles at different 3-D dihedral angles.

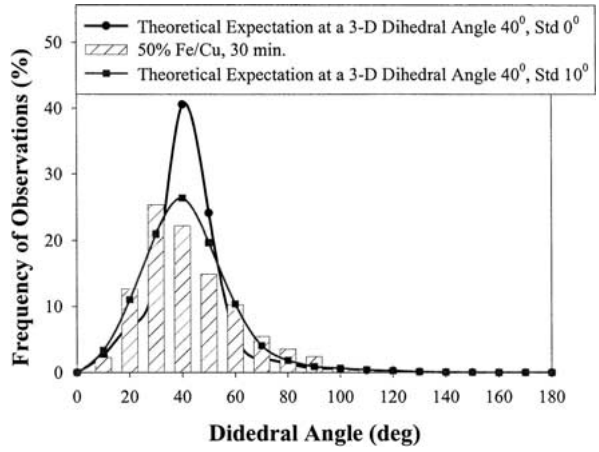

Figure 14 Expected 2-D dihedral angle distributions at a 3-D dihedral angle of 40° with standard deviations 0° and 10° compared with the experimental 2-D dihedral angle distributions with a composition of 50 vol% Fe/Cu for the sintering time of 30 min.

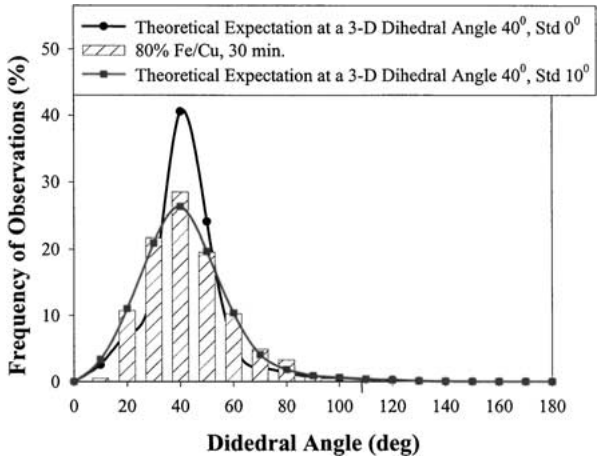

Figure 15 Expected 2-D dihedral angle distributions at a 3-D dihedral angle of 40° with standard deviations 0° and 10° compared with the experimental 2-D dihedral angle distributions with a composition of 80 vol% Fe/Cu for the sintering time of 30 min.

TABLE I Calculated χ^2 values for the current model and experimental distributions

Compositions	Sintering times	χ^2	Compositions	Sintering times	χ^2
50 vol%	20 min.	9.28	70 vol%	20 min.	5.96
Fe/Cu	30 min.	8.53	Fe/Cu	30 min.	9.30
	60 min.	18.67		60 min.	11.67
	330 min.	24.57		330 min.	6.52
60 vol%	20 min.	12.00	80 vol%	10 min.	7.56
Fe/Cu	30 min.	13.79	Fe/Cu	30 min.	5.54
	60 min.	10.69		60 min.	8.26
	330 min.	17.70		40 min.	8.15

The goodness of fit of the theoretically expected 2-D dihedral angle distribution based on the current model to the distribution of experimentally measured dihedral angles for various solid volume fractions of microgravity liquid phase sintered Fe-Cu samples is presented in Figs 14 and 15. The theoretical distribution for a single unique 3-D dihedral angle, that is 40° in our case, doesn't yield a satisfactory match to the experimentally observed distributions as reported by other researchers [7, 8]. Good agreement between the theoretical distribution for a normal distribution of 3-D dihedral angles around 40° with a standard deviation of 10° and the experimental data was obviously shown in Figs 14 and 15. The goodness of fit of the experimental and expected distributions was tested by the chi-squared test. The equation for the chi-squared test is [12]

$$\chi^2 = \sum_{i=1}^{k} \frac{(y_i - e_i)^2}{e_i} \tag{58}$$

where k is the number of intervals the results were grouped into, y_i is the measured number in the interval, e_i is the expected value of y_i predicted by the model. The degrees of freedom are $v = k - 1 = 17 - 1 = 16$. The critical value is $\chi^2_{0.005,16} = 26.296$. The model is rejected if this critical value is exceeded. Comparison of the calculated values of χ^2 (Table I) to this critical value concludes that the measured experimental dihedral angle distributions in all the sixteen microgravity processed Fe-Cu specimens may be modeled by the theoretical prediction at a 3-D dihedral angle of 40° with a standard deviation of 10°. The variance in 3-D dihedral angle may arise from the lack of geometric equilibrium, or from varying grain boundary energy with misorientation, or from orientation factors [7], or even from measuring error [8]. As we can see in Fig. 1, the solid grains are not perfectly spherical. The shape factor of the solid grains could cause this variance, too.

The current distribution calculated with a 3-D dihedral angle of 120° was compared with the distribution data provided in [6] in Fig. 16. Both Harker's data (Skewness = −1.17) and our data (Skewness = −1.56) skewed to the left, but Harker's data have a lower peak, while our data has a higher peak. The chi-squared test between these two sets of data using Harker's data as expected frequencies showed that the computed $\chi^2 = 19.04$ is well below the critical value

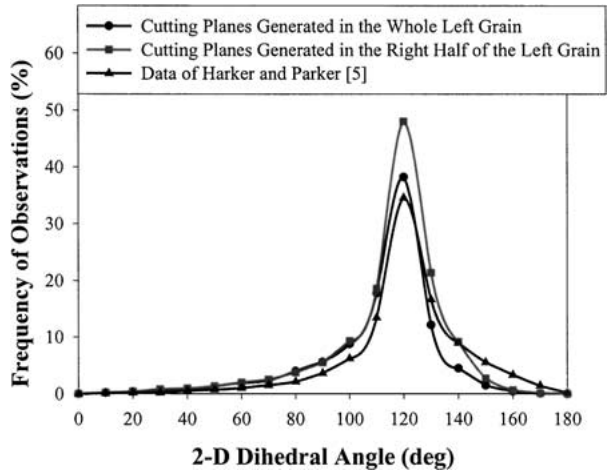

Figure 16 Comparison of expected distribution of Harker and Parker to the data of the current model at a 3-D dihedral angle of 120°.

$\chi^2_{0.05,18} = 28.9$. This means that no significant difference exists between them although their peak occurrence, skewness is not the same. The data collected in our microgravity processed Fe-Cu samples have a higher distribution of smaller angles as shown in Figs 14 and 15, that feature of distribution fits a model with higher left skewness. Our model and simulation were justified.

5. Conclusion

A new dihedral angle model was developed to statistically simulate the 2-D dihedral angle distribution and to obtain the corresponding 3-D dihedral angle. Simulations based on this model show that the grain size distribution has no effect on the 2-D expected dihedral angles. The relation between the 2-D expected dihedral angle and the 3-D dihedral angle is $\gamma = \frac{14}{15}\phi$. The normal distributed 3-D dihedral angle of 40° with a standard deviation of 10° fits the experimentally measured data, while the distribution expected from a unique 3-D dihedral angle of 40° has a much higher peak and narrower expansion than the experimentally measured distribution for all 16 Fe-Cu microgravity processed specimens.

Acknowledgment

This work was supported by NASA under cooperative agreement NCC8132 to the Consortium for Materials Development in Space at The University of Alabama in Huntsville. Engineering support was also provided by NASA and Lockheed Martin. Numerous individuals from academia, industry and government lent their knowledge, cooperation and support throughout this project.

References

1. R. M. GERMAN, *Metall. Trans. A* **18A** (1987) 909.
2. E. E. UNDERWOOD, in "Quantitative Stereology" (Addison-Wesley, Reading, MA, 1970).
3. H. E. EXNER, *Inter. Metall. Rev.* **17** (1972) 25.

4. Y. LIU, R. M. GERMAN and R. G. IACOCCA, *Acta Mater.* **47** (1999) 915.
5. R. M. GERMAN, in "Liquid Phase Sintering" (Plenum Press, New York, 1985).
6. D. HARKER and E. PARKER, *Trans. ASM* **34** (1945) 156.
7. CH. A. STICKELS and E. E. HUCKE, *Metall. Soc. AIME, Trans.* **230** (1964) 795.
8. S. R. JUREWICZ and A. J. G. JUREWICZ, *J. Geophys. Res.* **91** (1986) 9277.
9. O. K. RIEGGER and L. H. VAN VLACK, *Metall. Soc. AIME, Trans.* **218** (1960) 933.
10. J. NASER, J. E. SMITH JR. and A. K. KURUVILLA, *J. Mater. Sci.* **33** (1998) 5573.
11. R. T. DEHOFF, *Metallography* **19** (1986) 209.
12. S. DOWDY and S. WEARDEN, in "Statistics for Research" (John Wiley and Sons, New York, NY, 1983).

Received 15 August 2000
and accepted 25 February 2002